Measurement 244 (2025) 116475

Contents lists available at ScienceDirect

Measurement

journal homepage: www.elsevier.com/locate/measurement

Subsea pipeline spanning detection using a spherical detector with AC magnetic proximity switches

Yuan Wang [a,1], Jialin Wang [a,1], Jinyu Ma [a], Jian Li [a], Xinjing Huang [a,b,*]

[a] State Key Laboratory of Precision Measurement Technology and Instruments, Tianjin University, Tianjin, China
[b] Guangxi Key Laboratory of Automatic Detecting Technology and Instruments, Guilin University of Electronic Technology, Guilin, Guangxi, China

ARTICLE INFO

Keywords:
Pipeline spanning
Pipeline bending
Inclination
Proximity switch
In-pipe detection

ABSTRACT

Spanning and bending of subsea pipelines seriously threatens pipeline transportation safety. Traditional external detection methods based on underwater robots of pipeline spanning have high costs and low detection efficiency; internal detection methods such as Pipeline Inspection Gauges (PIGs) have high blockage risk and can only provide very low frequent inspection. In order to facilitate and effectively detect subsea pipeline spanning, this paper proposes a spanning and bending pipeline inclination measurement based on in-pipe spherical detector (SD) and AC magnetic proximity switches (ACMPSes). It has the advantages of low blockage risk, high precision, low cost and being quasi real-time. Through off-line data processing, the pipeline inclination is calculated by using the tangential and normal accelerations when the ACMPS reaches the extreme point to determine the degree of pipeline spanning and bending. The operation circuit and SD of the ACMPSes are developed. Experiments are carried out in a 24 m long, 8 in. steel pipe that naturally downward bends. Results demonstrate that the SD can autonomously realize fixed-axis rolling driven by the water flow in the pipeline, and the repeated measurements under different flow velocities have high accuracy and good consistency. Within ±2°, the average error of single measurement is 0.14°–0.31°. After the fusion of multiple measurements, the maximum error is 0.21° and the average error is 0.12°, which proves the effectiveness and accuracy of this method.

1. Introduction

In recent years, with the rapid development of subsea oil and gas exploitation all over the world, the length of subsea pipeline has quickly increased. Meanwhile, its safety problem has become increasingly prominent. Due to the scouring effect of ocean current and the seabed movement and unevenness, subsea pipeline spanning may occur. Without underneath foundation support, the subsea pipeline will sag and bend under the gravity [1,2]. Pipeline spanning will continuously develop under the erosion of ocean current, and the bending stress of the pipeline will also increase. Once the stress exceeds the bearing limit, the pipeline will break, resulting in huge economic losses and serious environmental pollution [3]. The free spanning subsea pipeline is shown in Fig. 1. Therefore, timely and accurate detection of subsea pipeline spanning and bending is of great significance for the maintenance and long-term safe operation of subsea pipelines.

At present, subsea pipeline inspection is mainly divided into external method and internal method. The external inspection method includes Remotely Operated Vehicle (ROV) and Autonomous Underwater Vehicle (AUV). The internal inspection method includes Pipeline Inspection Gauges (PIG) and spherical detector (SD).

The underwater robots - ROV and AUV are used in the low-frequency inspection of subsea pipeline. The detection principle is shown in Fig. 2. They can carry a variety of detection equipment, such as underwater camera, sonar, magnetometer, etc. ROV and AUV break through the depth limit of human diving, travel along the subsea pipeline and record its location, in situ state, and real-time images, which can be used to detect exposing, spanning, leak and other states of subsea pipelines [5–7]. The ROV has a limited operating range due to the limitation of umbilical cables [8]. The AUV does not have the limitation of umbilical cables, but it has high requirements for real-time data processing and control performances [9,10]. The AUV scans the seafloor in large areas along the preset zigzag trajectory and records the data for offline processing with high blindness and low efficiency [10]. However, underwater robots are deployed with high cost, because surface mother ship is required to cooperate with ROV and AUV, so the inspection cycle is very

* Corresponding author at: State Key Laboratory of Precision Measurement Technology and Instruments, Tianjin University, Tianjin, China.
E-mail address: huangxinjing@tju.edu.cn (X. Huang).
[1] Yuan Wang and Jialin Wang contributed equally to the work.

https://doi.org/10.1016/j.measurement.2024.116475
Received 18 November 2023; Received in revised form 5 November 2024; Accepted 9 December 2024
Available online 10 December 2024

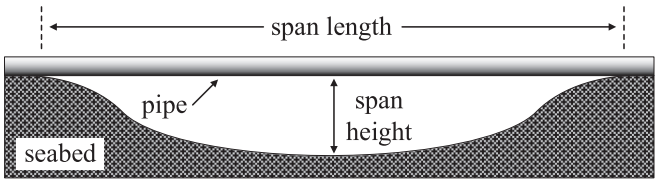

Fig. 1. Schematic diagram of the free spanning subsea pipeline (modified from [4]).

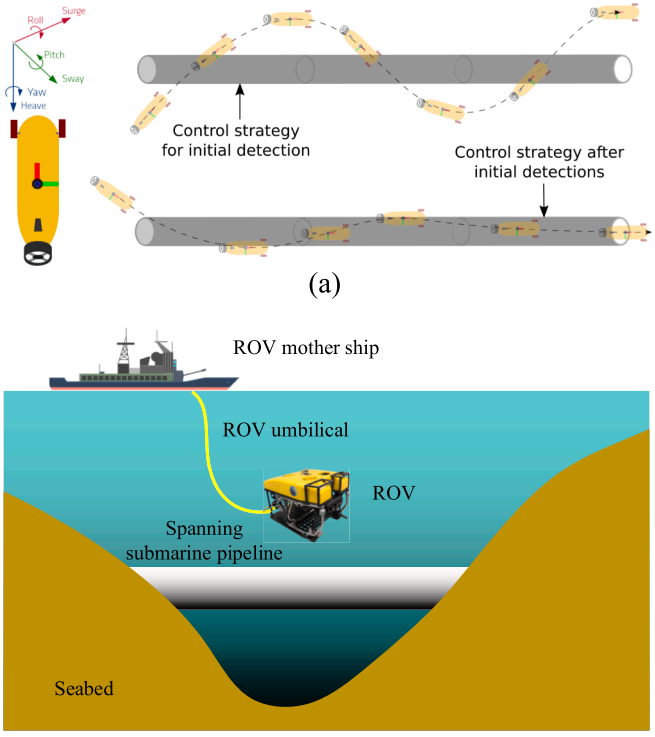

Fig. 2. Schematic diagram of pipeline external inspection methods. (a) AUV [11]; (b)ROV.

long. In addition, this kind of method is susceptible to the complex environment of the ocean.

The internal inspection method for subsea pipelines has the advantages of high detection efficiency, no restriction from the external environment, and low cost. The detection principle is shown in Fig. 3. At present, the PIG has been widely used in the inspection of onshore pipelines, but its application in subsea pipelines is limited because of its large size and the high risk of blockage when traveling in the pipeline as the PIG tightly contacts the inner pipe wall [12]. The in-pipe PIG has relatively low detection cost compared to ROV and AUV. PIG can use magnetic flux leakage or ultrasound to detect corrosion defects and cracks and can use inertial navigation system to measure the geographic coordinates of the pipeline. Since the PIG is relatively large in mass, it

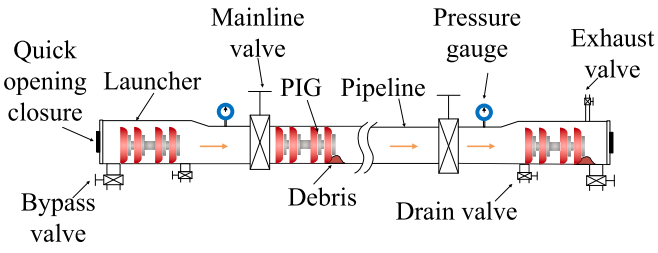

Fig. 3. Schematic diagram of pipeline internal inspection method PIG [15].

will affect the deflection of the pipeline when passing through the spanning pipeline [13], causing shaking and other problems. However, the buried pipeline has external soil environment support and can better fix the pipeline [14], so the PIG is more suitable for the positioning and defect detection of buried pipelines. Also, the PIG cannot be deployed frequently and cannot conduct quasi real time detection. However, spanning and bending of subsea pipelines is caused by seawater erosion, which changes rapidly and requires quasi real time detection.

In addition to the above solutions using internal and external detectors, pipeline monitoring solutions based on distributed fiber optics or piezoelectric devices have also been proposed in recent years to sense pipeline deformation, defect and vibration [16–18]. The detection principle is shown in Fig. 4. The distributed optical fiber method has high detection accuracy and low cost, but it is necessary to lay optical fiber on the outer wall of the pipeline when the pipeline is laid. It is very difficult to lay pipelines and optic fiber at sea at the same time. With the increasing of using time, the optic fiber has creep and high risk of being broken by an external force.

Due to the inconvenience of the above detection methods, our research group proposed a new pipeline defect detection solution based the SD. The diameter of the SD is smaller than the inner diameter of the pipeline, so the SD can freely move under the push of the fluid in the pipeline and has high passing ability [21]. The SD has good application prospects in the field of subsea pipeline detection, including pipeline leak detection [22,23], pipeline positioning [24] and pipeline inclination measurement [25]. The detection principle is shown in Fig. 5. The SD is put into the pipeline from one end and rolls forward under the drive of the liquid flow in the pipeline. It has no risk of jamming because its diameter is smaller than the inner diameter of the pipeline. Also, it can be used for densely launching and quasi-real-time subsea pipeline spanning monitoring thanks to its great convenience of employment compared to traditional PIGs: costing much less time for launch and retrieve and moving faster than the PIG. Therefore, there are broad application prospects in the detection of the overhang degree of a single pipeline.

In recent years, a lot of research has proposed a series of detection methods for spanning pipeline shape and location information based on the SD [26–29]. X. Huang [30] used the SD to measure the geographic coordinates of pipeline, but the accuracy is too low to distinguish the vertical bending of the spanning pipeline. The rolling speed of the SD is used to detect the bending of the spanning/subsidence gas pipeline [31]. The SD rolling speed changes were measured by extracting the AC component spectrum and the DC component of the acceleration signal recorded by the SD. This method has been tested in air-filled pipelines, but not yet in liquid-filled pipelines. The thrust exerted on the SD in the liquid-filled pipeline is much greater than that exerted on the SD in the gas pipeline, so the rolling speed of the SD changes very slightly with the change of the pipeline inclination and the rolling speed of the SD cannot indicate the liquid-filled pipeline's vertical bending. A method of measuring the pipeline inclination angle based on magnetic proximity switch and accelerometer has been proposed in [32]. It requires

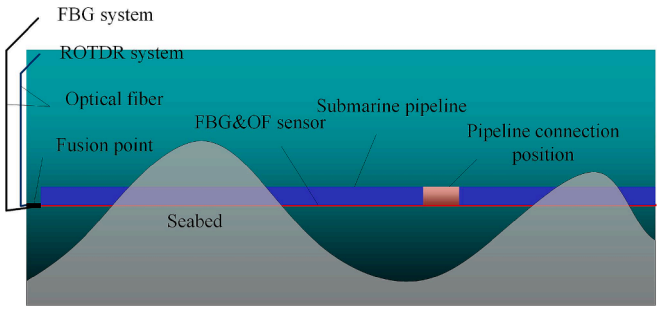

Fig. 4. Schematic diagram of pipeline external inspection method based on optical fiber (modified from [19,20]).

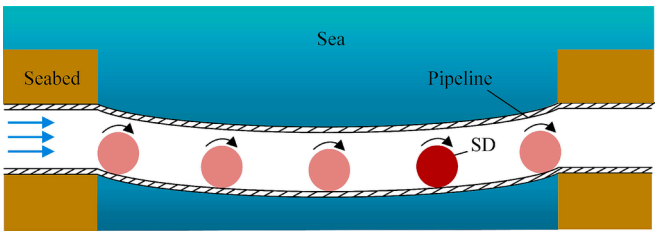

Fig. 5. Schematic diagram of pipeline internal inspection method based on the SD.

magnetizing the pipe wall with a small magnet that causes strong interference to the SD's magnetic sensor. The test was carried out by pushing the SD with a handle, which does not conform to the actual rolling scenario of the SD in the on-site pipeline [32]. Moreover, the lift-off value of this method is very small, and the sensor needs to be installed on the outer surface of the SD in order to be close to the pipe wall. This method has not been tested in actual liquid-filled pipelines. J. Li et al. [33] used the SD equipped with multi-channel magnetic sensors to detect the magnetic fields inside a pipeline to determine whether the pipeline is displaced or deformed. This method can only make qualitative judgments for large bending and cannot quantitatively evaluate the little inclination of the slightly bending pipeline.

The advantages and disadvantages of each method are comprehensively compared, and the results are shown in Table 1. In order to solve the shortcomings of the previous methods, this paper proposes a new measurement method of pipeline spanning state based on AC magnetic proximity switch (ACMPS) and accelerometer installed in the SD, which has the advantages of not interfering with the magnetic field in the pipeline, high lift-off value and high precision. First, this paper designs the measurement scheme of the SD, including structure, algorithm, circuit, acquisition and storage, etc. Second, the ACMPS is developed and its function is verified via both finite element simulation and experiment. Third, the newly developed SD equipped with elaborate ACMPS array and counterweight is successfully employed to measure the inclination of a 24 m long, 8 in. spanning bent steel pipeline. Lastly, measurement results and measurement accuracy are discussed and analyzed.

2. Measurement scheme

The measuring device consists of a SD and six ACMPSes based on RLC (Resistor-Inductor-Capacitance) resonance, as shown in Fig. 6. The SD carries six detection coils and a three-axis accelerometer. The accelerometer is located at the center of the SD, and the direction of the sensitive acceleration axis is aligned along the vector from the coil center to the SD center in order to obtain the radial and tangential components of the gravitational acceleration.

The detection coils are fed with high-frequency alternating current. The coils are connected in series into RLC resonant circuits as the inductors. When the detection coil in the SD is far away from the wall of the ferromagnetic pipe, the equivalent circuit diagram is shown in Fig. 7 (a). The circuit is an RLC oscillation circuit, and the circuit impedance is

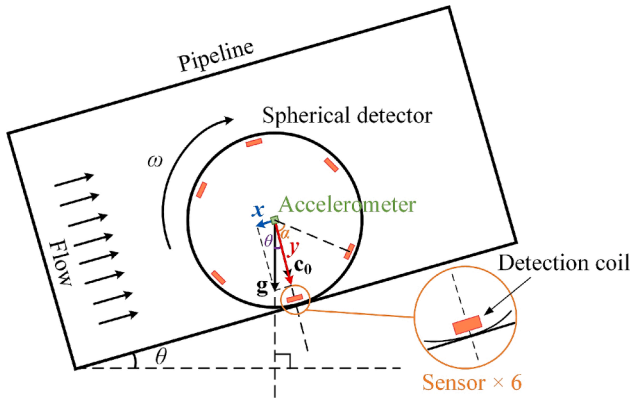

Fig. 6. Principle of pipeline inclination measurement.

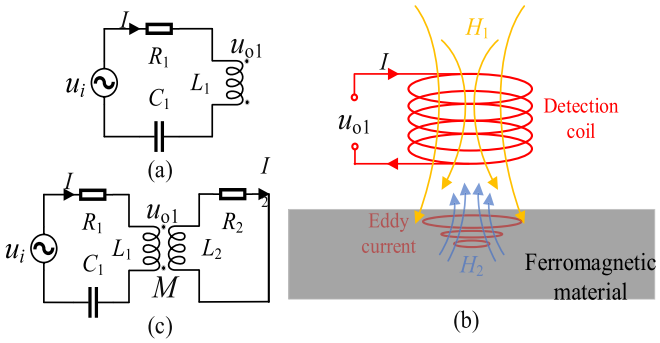

Fig. 7. Eddy current testing principle diagram. (a) RLC oscillation circuit diagram (without ferromagnetic material); (b) Schematic diagram of eddy current testing; (c) RLC equivalent circuit diagram (with ferromagnetic material).

shown in formula (1):

$$\begin{aligned} Z &= R_1 + j(X_L - X_C) \\ X_L &= \omega L_1 \\ X_C &= 1/\omega C_1 \end{aligned} \tag{1}$$

where R_1 is the resistance, X_L is the inductive reactance, X_C is the capacitive reactance, and w is the excitation angular frequency. When the excitation angular frequency of the voltage source is equal to the resonant frequency of the oscillation circuit, series resonance occurs and the voltage on the inductor L_1 will be amplified. The amplification factor depends on the R_1, L_1 and C_1. The voltage u_{o1} on the inductor L_1 is shown in formula (2):

$$\begin{aligned} Q &= \frac{1}{R_1}\sqrt{\frac{L_1}{C_1}} \\ u_{o1} &= j\omega_0 L_1 \frac{u_i}{R_1} = jQu_i \end{aligned} \tag{2}$$

where ω_0 is the resonant frequency, Q is the quality factor. According to

Table 1
Comparison of detection methods for subsea spanning pipeline.

Detection method	real-time evaluation	measurement range	resolution	sensitivity	accuracy	cost	others
Remote operated vehicle (ROV)	No	Limited	High	High	High	High	——
Autonomous underwater vehicle (AUV)	No	Large	High	High	High	High	Low detection efficiency
Pipeline Inspection Gauge (PIG)	No	Unlimited	Moderate	Moderate	High	Low	High jamming risk
Distributed fiber optics or piezoelectric devices	Yes	Limited	Low	High	Low	Low	Difficult construction
Spherical detector (SD)	being quasi real-time	Unlimited	High	High	High	Low	——

the conclusion in Reference [34], when the detection coil approaches the wall of the ferromagnetic pipe, eddy current is generated on the surface of the ferromagnetic pipe due to the primary magnetic field H_1 generated by the coil. The secondary magnetic field H_2 generated by the eddy current cancels out the primary magnetic field H_1. The schematic diagram is shown in Fig. 7(b). The equivalent circuit diagram is shown in Fig. 7(c). The shorter the distance between the detection coil and the ferromagnetic material, the greater the mutual inductance M. As the excitation frequency increases, the resistor R_2 is much lower than the inductive reactance ωL_2. Therefore, when the detection coil is closest to the pipe wall, the inductance value of the detection coil is represented by L_{steel}. L_{steel} can be approximately calculated by formula (3):

$$L_{steel} \approx L_1 - \frac{M^2}{L_2} \tag{3}$$

Therefore, when the detection coil is closest to the pipe wall, the equivalent mutual inductance M between the eddy current generated by the detection coil and the pipe wall is the largest, the inductance L of the detection coil becomes L_{steel}, the resonant frequency ω_0 of the circuit changes, the circuit impedance Z increases, the current I passing through the circuit decreases, and the inductive reactance X_L of the detection coil decreases, so the voltage u_{o1} on the coil decreases.

When the coil is closest to the inner wall of the pipe, the output voltage of the coil is minimum. At this moment, the line between the coil center and the SD center is perpendicular to the pipe wall, and this direction is $\mathbf{c}_0$. The direction of gravitational acceleration $\mathbf{g}$ always points downward to the center of the earth at any position. Therefore, according to the triangle similarity theory, the angle between $\mathbf{c}_0$ and $\mathbf{g}$ at this time is the pipeline inclination angle θ, which is expressed by formula (4).

$$\theta = \angle(\mathbf{g}, \mathbf{c}_0) = tan^{-1}(a_x/a_y) - \alpha \tag{4}$$

wherein, a_x and a_y are the outputs of the x axis and y axis of the accelerometer respectively, and α is the angle between the y axis of the accelerometer and the direction $\mathbf{c}_0$ parallel to the coil axis. For the first coil, the directions of y axis and $\mathbf{c}_0$ coincide, and α is zero.

In order to accurately capture the near-wall moment, it is necessary to ensure that the detection coils are on the mid-vertical plane of the SD, and the SD needs to do fixed-axis rolling in the pipeline. Therefore, the structure of the SD is redesigned in this paper. The internal composition and structural layout of the SD are shown in Fig. 8. The six-channel ACMPSes are excited by six resonant circuits, their voltage outputs are converted through the rectifier filter circuits and an analog digital converter, and then is stored in the TF card by the MCU together with the acceleration data. After the pipeline inspection is completed, the SD is taken out of the pipeline, and the recorded data is processed offline to calculate the pipeline inclination at each moment.

The average density of the SD is about 1.27 g/cm3, which is slightly larger than that of water. At the same time, the ratio of moment of inertia in three directions needs to meet $I_z/I_x = I_z/I_y \approx 1.55$, so as to realize the stable fixed-axis rolling of the SD in the pipeline. Six coils are evenly arranged on the mid-vertical plane of the SD, so when the SD rotates for one cycle, six values of pipeline inclination angle can be measured.

The SD uses tungsten cylinders for counterweight. Due to the high density of tungsten, small volume of tungsten cylinders can be enough to effectively control the mass distribution of the SD and save the limited space in the SD. According to reference [35], for a cylinder with radius r, mass m, and height h, as shown in Fig. 9, its moment of inertia is:

$$\begin{aligned} I_x = I_y &= \frac{1}{12} m(3r^2 + h^2) \\ I_z &= \frac{1}{2} mr^2 \end{aligned} \tag{5}$$

and the ratio of the two is:

$$\eta = \frac{I_z}{I_x} = \frac{I_z}{I_y} = \frac{6r^2}{3r^2 + h^2} \tag{6}$$

It can be seen that when $r \gg h$, η is maximum and the limit value is 2. Currently, the radius of the counterweight is much larger than its height, and the cylinder is disk-shaped. At this time, the stable rotation axis of SD is uniquely determined to be the circle with the largest moment of inertia. However, the complete counterweight is not easy to assemble and takes up too much space. Therefore, a circle of tungsten cylinder array is evenly arranged on the inner side of the spherical shell and on the mid-vertical plane of the SD. The diameter of the SD is 170 mm, which is less than 80 % of the diameter of the experimental pipeline to maintain high passability. It is with an average density of about 1.2 g/cm3 and a moment of inertia ratio of $I_z/I_x = I_z/I_y \approx 1.55$. This shows that SD can realize the stable fixed-axis rolling within the pipeline.

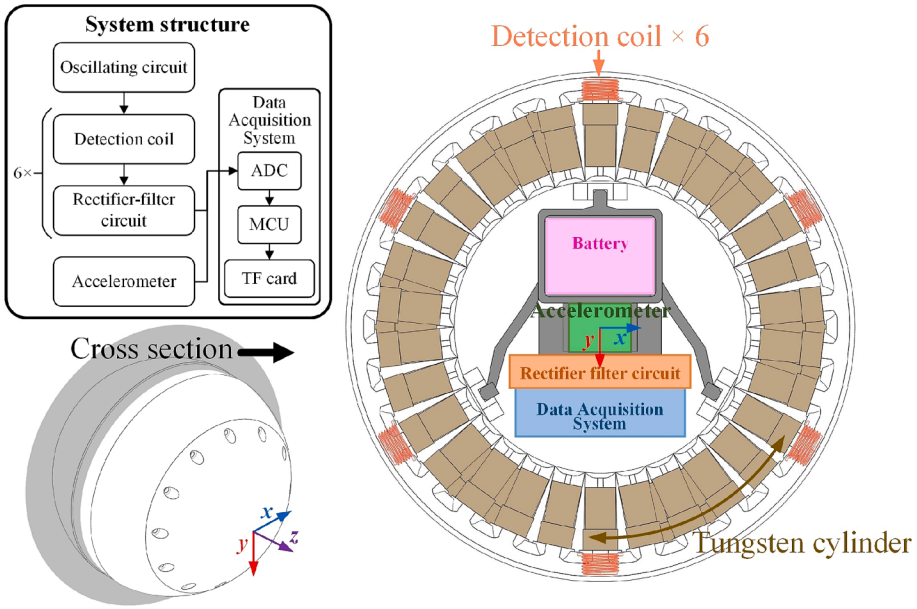

Fig. 8. System composition and cross section of the SD.

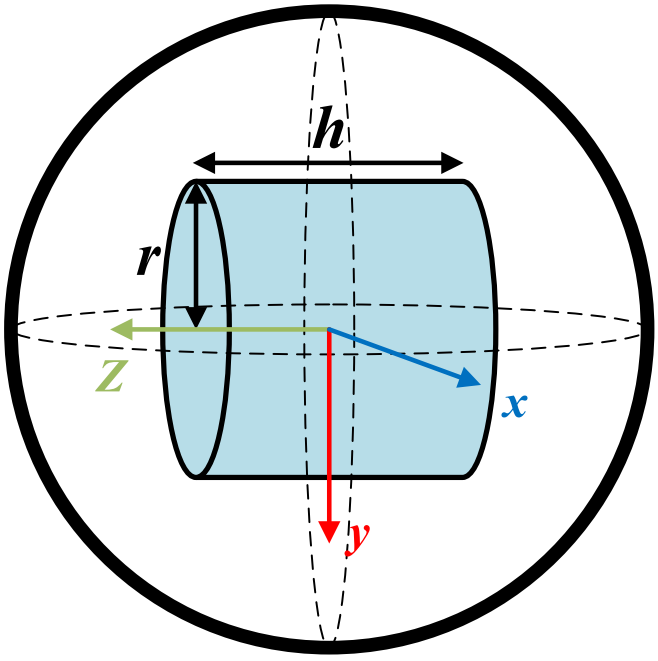

Fig. 9. Cylindrical counterweight model.

3. ACMPS and its function verification

ACMPS based on RLC(Resistor-Inductor-Capacitance) resonance principle is designed to sensitively detect the moment when the coil is closest to the pipe wall. According to the principle of RLC series resonance, when the excitation frequency is equal to the resonance frequency, the voltage of L_1 will be several times of the excitation voltage. The resonant frequency is $f = 1/(2\pi\sqrt{L_1 C_1})$. Because of eddy current effect, when the detection coil is close to the metal surface, the metal surface will generate inductive eddy current that has reaction on the coil. The induced eddy current forms an additional magnetic field, which prevents the magnetic field of the coil from alternating and attenuates the RLC resonance. The coil parameters will also change and the output voltage of the detection coil will decrease. Therefore, changes in the distance between the coil and the metal surface can be detected according to the changes in the output voltage.

3.1. Simulation verification

Finite element simulation software COMSOL Multiphysics is used to verify the feasibility of the ACMPS. The simulation model is shown in Fig. 10. The coil which is connected to a resonant circuit moves in a circle over the steel plate. The rotation radius of the probe is $r = 76.5$ mm, which is the same to the SD radius. φ is the rotation angle, the closest distance between the coil and the plate is $h = 6mm$, and the thickness of the steel plate is $d = 5mm$. In the circuit, the amplitude of excitation voltage u_i is 1 V, and the series resistance $R_1 = 1694\Omega$, the series capacitor $C_1 = 67.5pF$. When the coil is far away from the steel plate, $L_1 = 125.9mH$, and $R_{L_1} = 1.27k\Omega$. The excitation frequency is set as $f = 1/(2\pi\sqrt{L_1 C_1}) = 54.60$kHz, and the quality factor of the resonant circuit is $Q = \sqrt{L_1/C_1}/(R_1 + R_{L_1})^2 = 14.57$.

When the circuit is resonant, the waveform of excitation voltage u_i and coil's output voltage u_{o1} is shown in Fig. 11, and the coil voltage is significantly greater than the excitation voltage. When the coil is close to the steel plate, the eddy current weakens the resonance effect and reduces the voltage of the coil. Therefore, the minimum point of the coil voltage amplitude corresponds to the moment when the distance between the coil and the steel plate is the shortest.

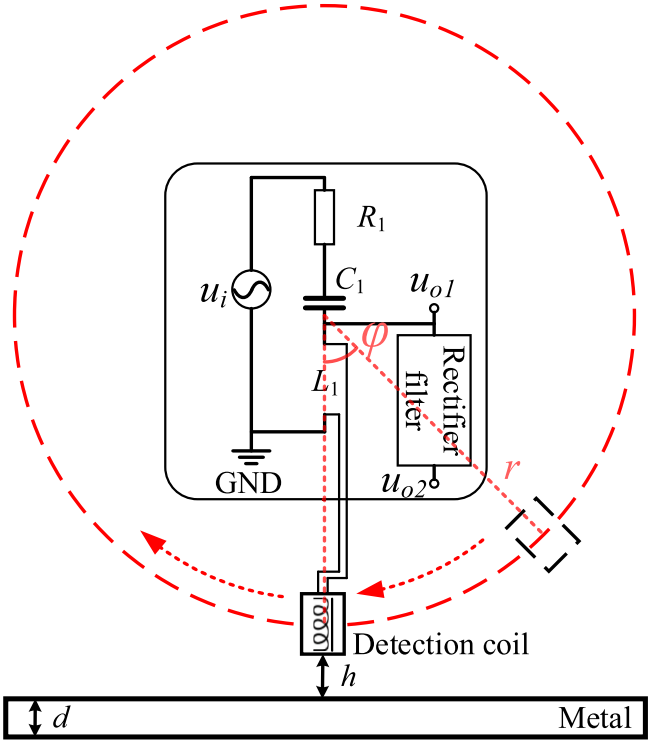

Fig. 10. Finite element simulation model.

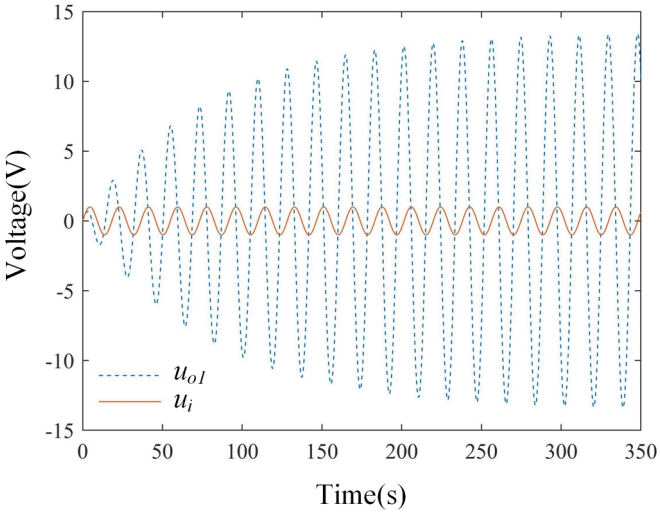

Fig. 11. Waveforms of excitation voltage and coil voltage when LCR resonance occurs.

By changing the rotation angle φ of the ACMPS, the amplitude of the output voltage u_{o2} and related parameters of the coil consequently change, as shown in Fig. 12. Fig. 12(a) shows the variation of the coil voltage amplitude u_{o2} with the change of φ. Fig. 12(b) shows the variation of the coil inductance L_1. Fig. 12(c) shows the variation of the coil

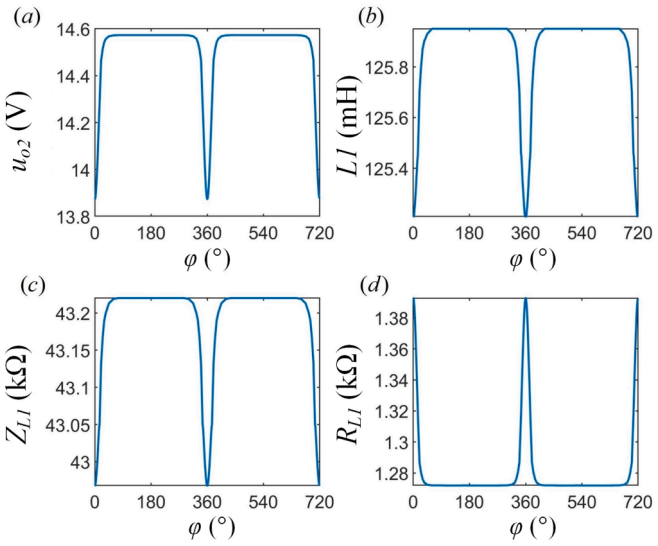

Fig. 12. Variation of coil parameters with the change of φ: (a) output amplitude u_{o2}; (b) coil inductance L_1; (c) coil impedance Z_{L_1}; (d) coil AC resistance..R_{L_1}

impedance Z_{L_1}. Fig. 12(d) shows the variation of the coil resistance R_{L_1}. It can be seen that when the coil rotation angle φ is 0° / 360° / 720°, namely, when the coil is closest to the steel plate, all the relevant parameters of the coil appear extreme values. It proves that it is practical to use the RLC resonance principle to determine the closest distance between the coil and the steel plate. Considering that voltage measurement is more convenient and accurate, u_{o2} will be used as the characterization variable of the proximity point. When the coil is closest to the pipe wall, the extreme point of u_{o2} appears. The acceleration signal at this moment is used to calculate the angle between the gravity and the line from the coil center to the SD center, which is also the pipeline inclination angle.

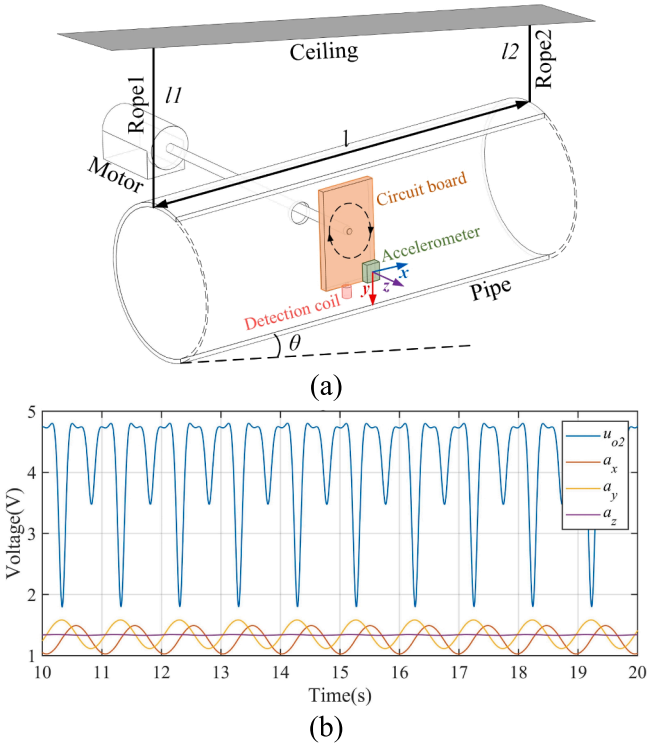

Fig. 13. Verification experiment of ACMPS function: (a) schematic; (b) output data of measurement system.

3.2. Experimental verification

The pipeline spanning state detection method based on the ACMPS is verified under laboratory conditions using the experimental scheme as shown in Fig. 13(a). The length of the steel pipe is l, and the pipe is hung on the ceiling by two wire ropes. The inclination angle of the pipe is adjusted by changing the lengths $l1$ and $l2$ of the wire ropes. The inclination angle of the pipe is $\theta = \sin^{-1}(l1 - l2)/l$. The detection coil system is rotated in the steel pipe driven by a motor to simulate the rolling of the SD in the pipeline. The distances from the rotation axis to the top and bottom of the pipe are different. The measured acceleration and the waveform of u_{o2} are shown in Fig. 13(b). It can be seen that for each cycle of rotation, u_{o2} has two obvious extreme points, of which the larger one corresponds to the moment when the coil is closest to the bottom wall of the pipe (6 mm) and the smaller one corresponds to the moment when the coil is closest to the top wall of the pipe (11 mm).

The phenomenon that there is still a noticeable extreme point of u_{o2} with the lift-off value of 11 mm proves that this method has solved the problem of low lift-off value in the previous method previously proposed [32]. As the magnet being farther from the pipe wall, the magnetization of the pipe becomes weaker and the magnetic field change becomes smaller. If the distance is too close, the Hall sensor may reach saturation. The results of the inclination angle calculated according to the formula (1) are listed in Table 2. The maximum error is 0.23° in the range of 0~45° inclination angle, which confirms the feasibility and practicality of the proposed method.

Table 2
Verification experiment results of ACMPS function.

Actual θ (°)	Measured θ (°)	Error (°)
0.48	0.62	0.14
−3.63	−3.82	−0.19
−4.68	−4.79	−0.11
−7.47	−7.51	−0.04
−14.87	−14.94	−0.07
−17.46	−17.23	0.23
−26.49	−26.55	−0.06
−33.03	−32.98	0.05
−37.71	−37.70	0.01
−45.10	−45.11	−0.01

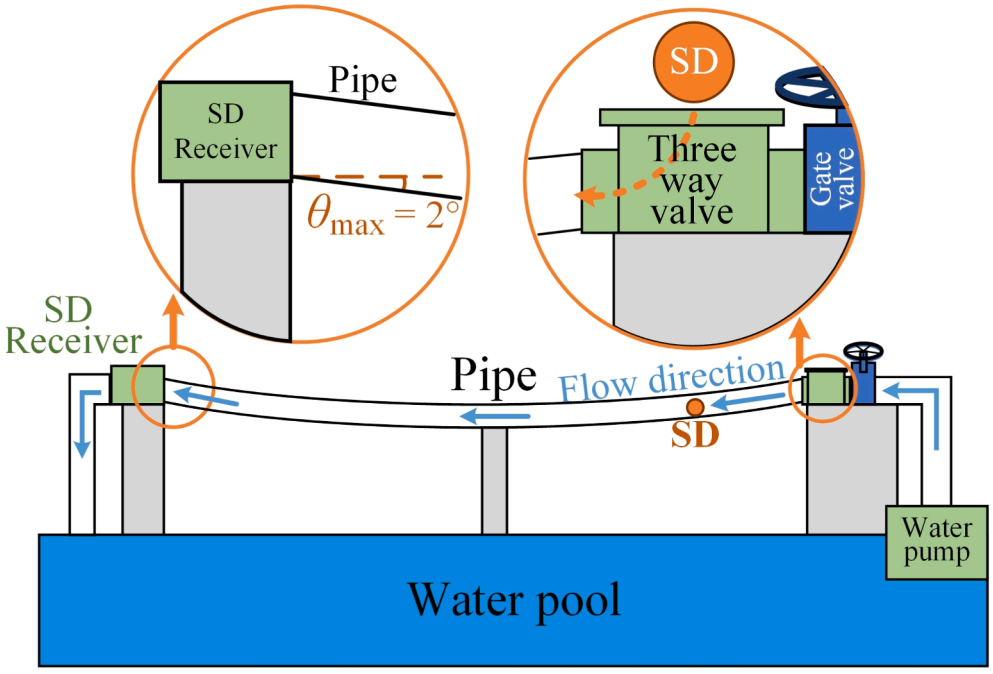

(a)

(b)

Fig. 14. Experimental pipeline system: (a) structural schematic; (b) photo of experiment field.

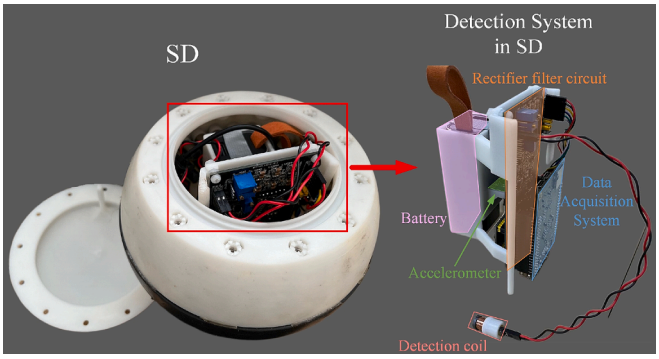

Fig. 15. SD used in the experiment.

4. Measurement experiment of spanning pipeline inclination

The pipeline system for application experiment is shown in Fig. 14. The SD used for the experiment is shown in Fig. 15. A 24 m long water delivery experimental pipeline was built. The pipe was made of carbon steel, with a diameter of 8 in., and a wall thickness of 6 mm. The two ends of the steel pipe were raised and fixed, causing the middle section to sag under gravity, simulating the inclination angle change when the subsea pipeline spanning and bending occurs. Water was pumped from the pool, and the water flow pushed the SD to roll forward. There was a three-way valve at the right end of the pipe to launch the SD, and a tank at the left end of the pipe to retrieve the SD. Besides, the water flow speed was adjusted by a gate valve between the three-way valve and the water pump. The actual inclination angle distribution of the steel pipe is shown in Table 3. The data was obtained by mechanical finite element simulation. The simulation model adopts 1:1 real size and real material parameters.

The SD was put into the three-way valve and then the cover was closed. The water pump was started and the SD rolled forward and finally rushed out from the other end of the pipe together with the water flow. Fig. 16 shows the acceleration data recorded by the SD while rolling in the pipe, from which we can see that the frequency and each component of the acceleration signals is steady, indicating that the SD's rolling speed and state is stable. The amplitudes of the two acceleration components are unfluctuating, indicating that the rotation axis of the SD is also stable. The above information proves that the SD with well-designed counterweight realizes stable fixed-axis rolling in the pipeline. By calculating the product of the SD's rolling frequency and circumference, the speed of the SD in water filled pipeline can be obtained. The gate valve at the right end of the pipeline was adjusted to control the flow velocity to have different values and test the moving speeds of the SD rolling in the pipeline respectively. The calculated rolling speeds of the SD are shown in Fig. 17. It can be seen that the SD rolls unstably due to the unstable flow in the initial stage, and the measured rolling speed fluctuates greatly in the initial stage. However, the SD quickly realizes fixed-axis rolling and its rolling speed in the pipeline quickly becomes stable. The SD's moving speed in the liquid-filled pipe mainly depends on the liquid flow velocity, and there is no obvious corresponding relationship between the rolling speed and the inclination angle of the spanning bent pipe. This also proves that the method of using the change of the SD's moving speed to detect the bending of pipeline proposed by [31] is no longer applicable to liquid-filled pipeline, which demonstrates the necessity of this method. This also solves the problem that the hand-held push rod drives the carrier to roll and cannot completely reproduce the rolling of the on-site spherical detector in the pipeline [32].

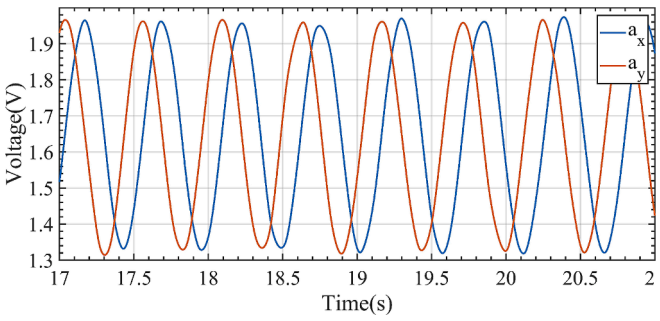

Fig. 16. Acceleration signals recorded by the SD rolling in the water flow pipe.

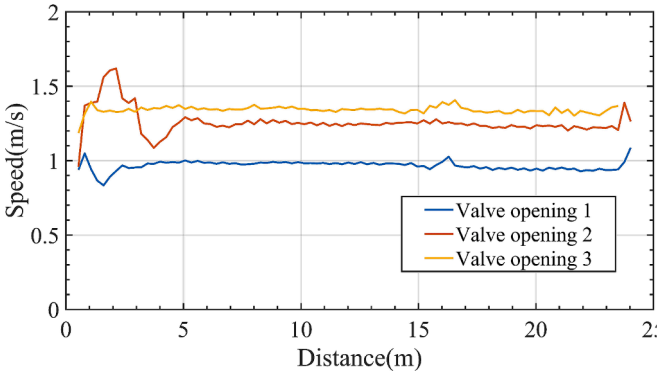

Fig. 17. Rolling speed of the SD at different flow velocity.

5. Results and discussion

The acceleration and ACMPSes' waveforms collected by the SD in the pipeline spanning detection experiment are shown in Fig. 18. It can be seen that in the water filled pipeline, the SD can stably roll around a fixed axis. The six channels of ACMPSes in each rolling cycle can effectively detect the changing distance between the detection coil and the pipe wall for six times. When the coil is closest to the pipe wall, the coil output amplitude reaches the extreme value. The peak detection algorithm is used to determine the minimum value and the moment of its occurrence, and the acceleration value a_x, a_y at this moment is used to calculate the pipeline inclination angle according to the formula (4). Then the six values of the pipeline inclination angle measured by six channels are averaged to provide the final measurement result in each rolling cycle.

Results of five repeated pipeline inclination measurements using the SD at a flow velocity of 0.95 m/s are shown in Fig. 19. The SD diameter is 170 mm and the average moving speed of the calculated SD is about 0.89 m/s. It can be seen that the results of multiple repeated experiments have good consistency. However, there are random errors in the data caused by disturbance in the process of the SD rolling. After using the average fusion of multiple measurement results, the measurement inclination angle is closer to the real value of the pipe. Because the SD can freely roll in the pipeline, the SD is not easy to get blocked and it is convenient to launch and retrieve. In field pipeline, the SD can be used

Table 3
Actual inclination angle of experimental pipeline.

Axial position (m)	1.00	3.00	5.00	7.00	9.00	11.00	13.00	15.00	17.00	19.00	21.00	23.00
Inclination angle (°)	1.98	1.85	1.57	1.20	0.75	0.25	−0.26	−0.75	−1.20	−1.57	−1.85	−1.98

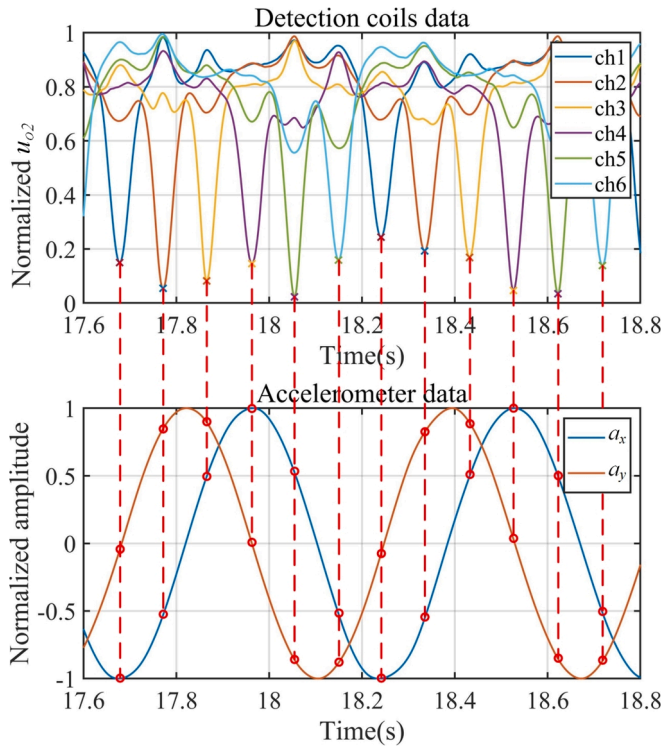

Fig. 18. A piece of data collected during pipeline inclination measurement experiments.

for repeated inspection to get the average value. This experimental result further proves the feasibility and practicality of the proposed method to measure the pipeline inclination angle.

It should be noted that there are large errors in the data of the initial and final sections due to the unstable water flow near the inlet and outlet of the experimental pipe that has resulted in the SD's unstable rolling and poor data quality. In the middle section of the pipe the water flow is more stable, so the quality of the data collected by the SD is higher and the error of the pipe inclination measurement is smaller. The field pipeline can be regarded as infinitely long, and the flow velocity and flow state in the pipeline are stable, so there will be no instability force to interfere with the rolling of the SD. Therefore, the detection accuracy of the SD in the field spanning/subsidence bent pipeline will be higher.

Because the inclination angle of the experimental pipeline is small, and the maximum angle is only 2°, the absolute error rather than the relative error is used for accuracy analysis. Error statistics of the inclination measurement results of the middle pipe section which is close to the field situation are done. The average errors of five measurements at the same flow velocity are 0.22°, 0.14°, 0.31°, 0.29° and 0.14° respectively. After taking the mean value of multiple experiment results, the maximum error is 0.21° and the average error is 0.12°. Therefore, for the field long-distance pipeline, the advantages of the SD that the SD is not easy to get blocked and is convenient to launch and retrieve should be made full use of, and the SD can be used to repeatedly inspect the pipeline to obtain accurate measurement results and realize quasi real-time detection of subsea pipelines.

The opening of the gate valve was adjusted to change the water flow velocity in the pipeline, and the measurement performance of the SD at different flow speeds was tested. The results are shown in Fig. 20. The pipeline inclination measurement results under different flow velocities are very close, and they all overlap the real inclination angle of the bending pipeline. This proves that the proposed method is insensitive to the liquid flow velocity in the pipeline, which is of great advantage. In the experiments with three different flow velocities, the average errors of the three measurements are 0.20°, 0.28°, and 0.28° respectively, which proves that this detection method has high accuracy and is not affected by variances in flow velocity.

The average moving speed of the calculated SD is about 0.89 m/s, so the SD won't take a long time to roll inside the long-distance pipeline. When the SD completes the pipeline detection, the pipeline inclination can be calculated immediately, and the degree of pipeline span can be judged. Therefore, the real-time performance of this method is better than others.

6. Conclusion

In this paper, a method of measuring the pipeline spanning detection based on ACMPS and accelerometer is proposed. This method can quantitatively detect the bending of a spanning pipeline. The main results are as follows:

(1) A new method for measuring the spanning state of subsea liquid filled pipelines is proposed. Under the action of fluid thrust, the SD rolls along the fixed axis in the pipeline, and the inclination of pipeline spanning is calculated by the collected acceleration data and the moment when the ACMPS is perpendicular to the wall of the ferromagnetic pipeline. Under laboratory conditions, the ACMPS is rotated by a motor to simulate the SD's rolling in the field pipeline to test the measurement accuracy, and the maximum inclination measurement error is 0.23° within the range of 0∼45°. Accurate inclination measurement can be achieved when the lift-off value is as far as 11 mm.

(2) A SD equipped with six ACMPSes for detecting the spanning state of subsea pipelines is designed. The layout of the ACMPS array in the SD, the multi-channel signal calculation circuit, and the data acquisition/storage module are developed. Six inclination measurements in each rolling cycle are achieved to ensure the sampling density and measurement accuracy. The structure layout and counterweight of the SD are designed to adjust the density distribution and moment of inertia of the SD, so that the SD can roll around a fixed axis in the liquid-filled pipeline.

(3) The proposed method is experimentally verified in a naturally sagging water-filled steel pipeline with a length of 24 m and a diameter of 8 in. The results show that the SD can autonomously realize fixed axis rolling under the impetus of water flow in the pipeline, and the repeated measurements of the pipeline inclination angle under different flow velocities have high precision and good consistency. Within the range of ±2°, the average error of single measurement is 0.14°∼0.31°. After fusion of multiple measurements, the maximum error is 0.21° and the average error is 0.12°.

CRediT authorship contribution statement

Yuan Wang: Writing – review & editing, Visualization, Formal analysis, Data curation, Software. **Jialin Wang:** Data curation, Methodology, Software, Writing – original draft. **Jinyu Ma:** Writing – review & editing, Project administration, Methodology, Investigation. **Jian Li:** Methodology, Conceptualization. **Xinjing Huang:** Writing – review & editing, Supervision, Project administration, Investigation, Funding acquisition, Conceptualization.

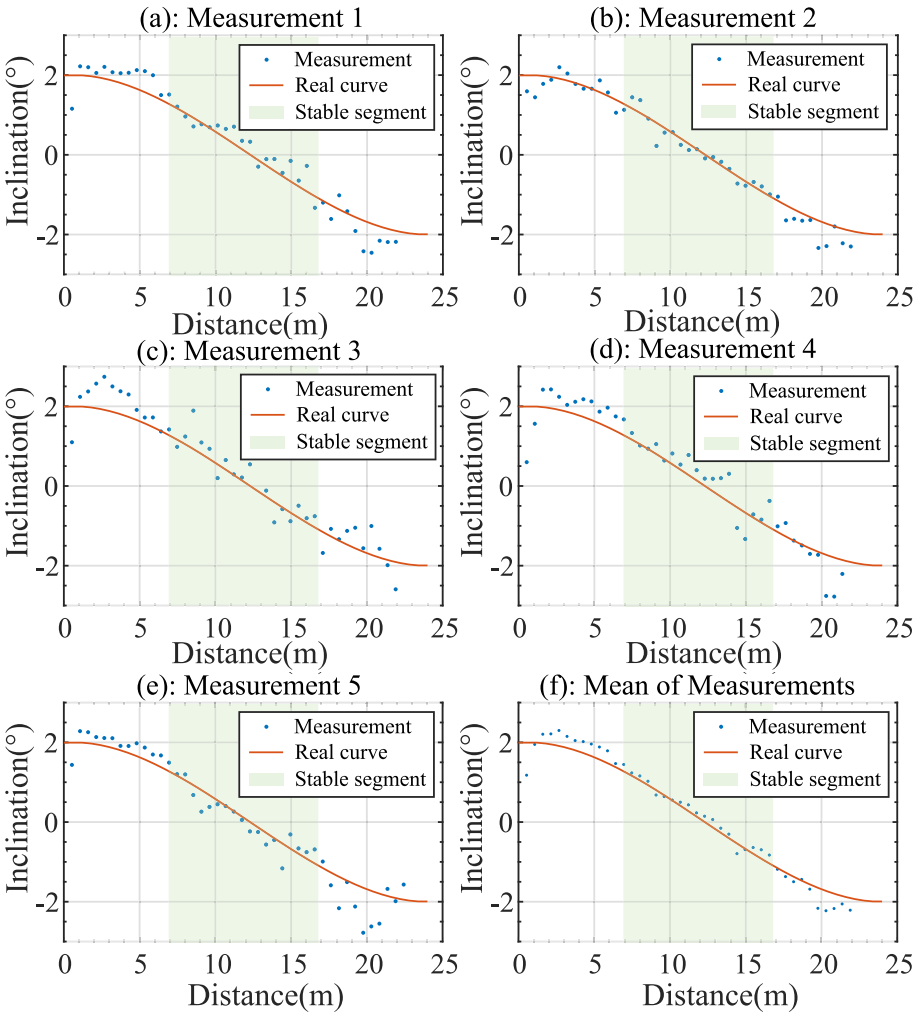

Fig. 19. Measurement results when the flow speed is 0.95 m/s: (a)-(e) single measurement result; (f) average value of multiple measurement results.

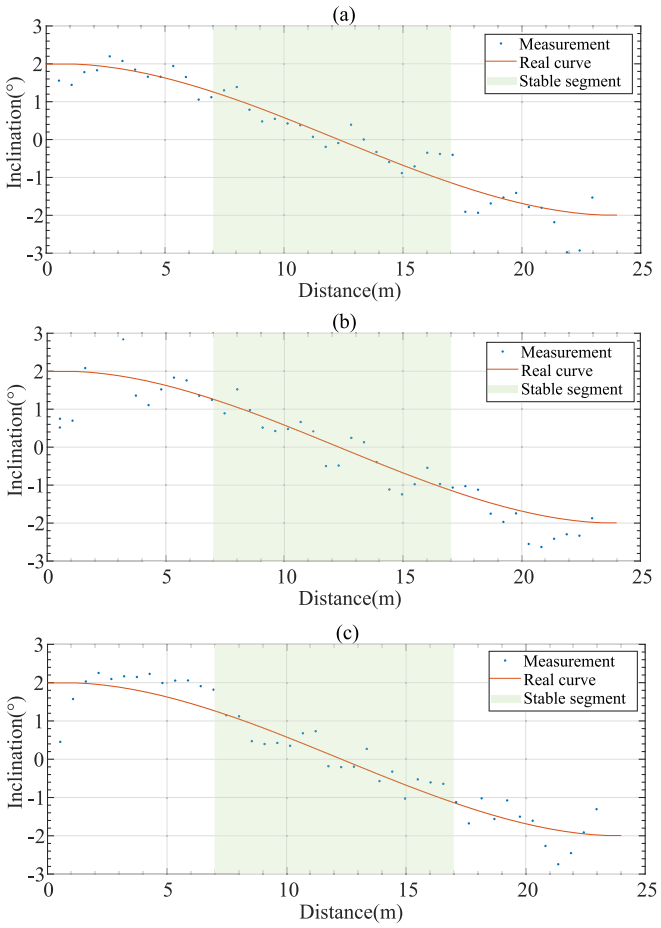

Fig. 20. Measurement results of the SD rolling with different speeds: (a)1.05 m/s; (b)1.25 m/s; (c)1.35 m/s.

Declaration of competing interest

The authors declare that they have no known competing financial interests or personal relationships that could have appeared to influence the work reported in this paper.

Acknowledgments

This work is supported by National Natural Science Foundation of China (Nos 62073233, 62473279) and Guangxi Key Laboratory of Automatic Detecting Technology and Instruments (No. YQ24203).

Data availability

Data will be made available on request.

References

[1] Y. Xie, X.F. Ma, H.F. Ning, Formation and damage mechanism of free spanning submarine pipeline, Oil & Gas Storage and Transport. 36 (12) (2017) 1436–1442, https://doi.org/10.6047/j.issn.1000-8241.2017.12.015.
[2] S. Goutam, R. Pronab, Effect of non-homogeneity of seabed soil on natural frequency of offshore free spanning pipeline, Lec. Notes in Civ. Eng. 188 (2022) 131–143, https://doi.org/10.1007/978-981-16-5673-6_11.
[3] X. Wei, Emergency collection and temporary storage environmental protection technology for underwater oil leakage during offshore oil exploration and development, Saf. Health & Environ. 19 (9) (2019) 25–28. CNKI: SUN: SAFE.0.2019-09-006.
[4] Y. Haryadi, M. Irfan, D. Muljawan, S. Ardhyastuti, Application of multibeam data for the identification of a possible free span on a subsea pipeline, Ocean Eng. Technol. Innov. Conf. (2022) 74–77, https://doi.org/10.1109/OETIC57156.2022.10176244.
[5] C. Sun, D. Zou, ROV-based deepwater pipeline external inspection technology, Pet. Eng. Constr. 45 (2) (2019) 1–5, https://doi.org/10.3969/j.issn.1001-2206.2019.02.001.
[6] B. Jia, J. Shuai, Y. Zhang, State detection and safety evaluation of submarine suspended pipeline, Oil & Gas Storage and Transport. 40 (6) (2021) 658–663, https://doi.org/10.6047/j.issn.1000-8241.2021.06.008.
[7] L. Paull, S. Saeedi, M. Seto, H. Li, AUV navigation and localization: a review, IEEE J. of Ocean. Eng. 39 (1) (2014) 131–149, https://doi.org/10.1109/JOE.2013.2278891.
[8] T. Wang, X. Peng, G. Pan, D. Xu, Development and key technologies of unmanned underwater vehicles, Astronaut. Syst. Eng. Technol. 1 (4) (2017) 52–64. CNKI:SUN:YHZJ.0.2017-04-009.
[9] A.V. Inzartsev, A.M. Pavin, AUV behavior algorithm while inspecting of partly visible pipeline, Oceans (2006) 1–5, https://doi.org/10.1109/OCEANS.2006.306793.
[10] S. Li, J. Liu, H. Xu, H. Zhao, Y. Wang, Research status of autonomous underwater vehicles in China, Sci. Sin. (Inform.) 48 (9) (2018) 1152–1164, https://doi.org/10.1360/N112017-00264.
[11] V. Bharti, D. Lane. and S. Wang, A Semi-Heuristic Approach for Tracking Buried Subsea Pipelines using Fluxgate Magnetometers, 2020 16th IEEE Intern. Conf. on Autom. Sci. Eng. (CASE). (2020) 10.1109/CASE48305.2020.9216755.
[12] M.H.W. Hendrix, H.P. IJsseldijk, W.-P. Breugem, R.A.W.M. Henkes, Experiments and modeling of by-pass pigging under low-pressure conditions, J. Process. Contr. 71 (2018) 1–13, https://doi.org/10.1016/j.jprocont.2018.08.010.
[13] M.H. Sadeghi, S. Chitsaz, M. Ettefagh, Effect of PIG's physical parameters on dynamic behavior of above ground pipeline in pigging operation, Mech. Syst. Signal Process. 132 (2019) 692–720, https://doi.org/10.1016/j.ymssp.2019.07.008.
[14] H. Liu, H. Zhang, X. Zhang, M. Chen, M. Gao, Theoretical research of impact vibration of multi-section serial pipeline inspection gauge in large drop pipeline, Eng. Fail. Anal. 162 (2024) 108430, https://doi.org/10.1016/j.engfailanal.2024.108430.
[15] Y. Cao, C. Liu, H. Tian, Y. Sun, S. Zhang, Mechanical behaviors of pipeline inspection gauge (pig) in launching process based on Coupled Eulerian-Lagrangian (CEL) method, Int. J. Press. Vessel. Pip. 197 (2022) 104622, https://doi.org/10.1016/j.ijpvp.2022.104622.
[16] X. Feng, W. Wu, X. Li, X. Zhang, J. Zhou, Experimental investigations on detecting lateral buckling for subsea pipelines with distributed fiber optic sensors, Smart Struct. Syst. 15 (2) (2015) 245–258, https://doi.org/10.12989/sss.2015.15.2.245.
[17] H. Lee, H. Sohn, Damage detection for pipeline structures using optic-based active sensing, Smart Struct. Syst. 9 (5) (2012) 461–472, https://doi.org/10.12989/SSS.2012.9.5.461.
[18] P. Cahill, V. Pakrashi, P. Sun, A. Mathewson, S. Nagarajaiah, Energy harvesting techniques for health monitoring and indicators for control of a damaged pipe structure, Smart Struct. Syst. 21 (3) (2018) 287–303, https://doi.org/10.12989/sss.2018.21.3.287.
[19] B. Liu, J. He, L. Zhang, J. Tang, S. Zhang, S. Zhang, Pipeline safety monitoring technology based on FBG-ROTDR joint system and its case study of urban drainage pipeline monitoring, Opt. Fiber Technol. 73 (2022) 103044, https://doi.org/10.1016/j.yofte.2022.103044.
[20] S. Zhang, B. Liu, J. He, Pipeline deformation monitoring using distributed fiber optical sensor, Meas. 133 (2019) 208–213, https://doi.org/10.1016/j.measurement.2018.10.021.
[21] S. Chen, C. Gao, S. Guo, X. Huang, Research on pass ability of spherical inner detector in vertical segment of submarine pipeline, Comput. Eng. Appl. 51 (19) (2015) 265–270, https://doi.org/10.3778/j.issn.1002-8331.1310-0112.
[22] Y. Li, Y. Zhou, M. Fu, F. Zhou, Z. Chi, W. Wang, Analysis of propagation and distribution characteristics of leakage acoustic waves in water supply pipelines, Sens. 21 (16) (2021) 5450, https://doi.org/10.3390/s21165450.
[23] T. Xu, Z. Zeng, X. Huang, J. Li, H. Feng, Pipeline leak detection based on variational mode decomposition and support vector machine using an interior spherical detector, Process Saf. Environ. Prot. 153 (2021) 167–169, https://doi.org/10.1016/j.psep.2021.07.024.
[24] X. Huang, S. Chen, S. Guo, T. Xu, Q. Ma, S. Jin, G.S. Chirikjian, A 3D localization approach for subsea pipelines using a spherical detector, IEEE Sens. J. 17 (6) (2017) 1828–1836, https://doi.org/10.1109/JSEN.2016.2586998.
[25] Y. Zhang, Y. Xue, X. Huang, J. Li, S. Chen, Characterizations of magnetic field distributions inside buckling pipelines, Appl. Comput. Electromagn. Soc. J. 33 (12) (2018) 1475–1482.
[26] X. Huang, G. Chen, Y. Zhang, J. Li, T. Xu, S. Chen, Inversion of magnetic fields inside pipelines: modeling, validations, and applications, Struct. Heal. Monit. 17 (1) (2018) 80–90, https://doi.org/10.1177/1475921716684563.
[27] L. Guo, Z. Zeng, X. Huang, J. Li, S. Chen, Vibration detection of spanning subsea pipelines by using a spherical detector, IEEE Access 7 (2019) 7001–7010, https://doi.org/10.1109/ACCESS.2018.2890024.
[28] W. Zhao, X. Huang, S. Chen, Z. Zeng, S. Jin, A detection system for pipeline direction based on shielded geomagnetic field, Int. J. of Press. Vessel. and Pip. 113 (1) (2014) 10–14, https://doi.org/10.1016/j.ijpvp.2013.11.001.
[29] X. Huang, Z. Li, Y. Zhang, Y. Xue, J. Li, Analyses and verifications of magnetic shielding of long pipelines aiming for pipeline orientation measurements, J. Magn. Magn. Mater. 517 (1) (2021) 167369, https://doi.org/10.1016/j.jmmm.2020.167369.
[30] X. Huang, Research on geographic coordinate measurement of subsea pipelines, Tianjin Univ. (2016), https://doi.org/10.7666/d.Y3174536.

[31] L. Guo, Z. Zeng, X. Huang, M. Li, H. Feng, J. Li, X. Rui, Low-cost and high-efficiency method for detecting vertical bends of subsea pipelines, IEEE Access 8 (2020) 33926–33933, https://doi.org/10.1109/ACCESS.2020.2974405.
[32] Y. Zhang, Y. Xue, X. Huang, J. Li, S. Chen, Pipeline inclination measurements based on a spherical detector with magnetic proximity switches, IEEE Access 6 (2018) 39936–39943, https://doi.org/10.1109/ACCESS.2018.2856618.
[33] J. Li, T. Liu, J. Wang, S. Liu, X. Huang, Internal detection of pipeline displacement and deformation based on magnetic sensor array, J. Electron. Meas. and Instrum. 38 (2) (2024) 76–84.
[34] G.Y. Tian, Z.X. Zhao, R.W. Baines, The research of inhomogeneity in eddy current sensors, Sens. Actuators, A. Phys. 69 (2) (1998) 148–151, https://doi.org/10.1016/S09244247(98)00085-5.
[35] L. Guo, Z. Zeng, X. Huang, et al., Performance enhancements of the spherical detector for pipeline spanning inspection through posture stabilization, Meas. 165 (2020) 108095, https://doi.org/10.1016/j.measurement.2020.108095.